OHIO STATE UNIVERSITY

The report from Ohio State for the period follows.

INTRINSIC FLOW BEHAVIOR IN A SLURRY BUBBLE COLUMN UNDER HIGH PRESSURE AND HIGH TEMPERATURE CONDITIONS

Quarter Report

(**Reporting Period:** January 1 to March 31, 1999)

Highlights

- The maximum stable bubble size in high-pressure slurry bubble columns was studied experimentally and analytically. The maximum bubble size decreases with an increase in pressure, and increasing solids concentration leads to larger bubbles. The particle effect is more significant at ambient pressure.

- A mechanistic model based on the concept of internal gas circulation inside a bubble was proposed to simulate the maximum stable bubble size in a high-pressure slurry bubble column. The mechanism and criterion of bubble breakup were illustrated by considering the internal gas circulation inside the bubble.

- Based on the model, an analytical expression was obtained to predict the maximum stable bubble size under high-pressure conditions. Comparison between the experimental data and model predictions showed that the proposed model can reasonably predict the maximum bubble size at elevated pressures.

Work Conducted

Experimental Study of Maximum Bubble Size
The bubble size and bubble size distribution in high-pressure slurry bubble columns can be measured by using an optic fiber probe, which was described in previous monthly reports (August - November, 1997). It should be noted that the probe can only measure the bubble chord length, and not the true bubble diameter. If a uniform bubble shape (either spherical or ellipsoidal) is assumed, the bubble chord length distribution can be converted to the bubble size distribution (Liu et al., 1996). However, bubbles in slurry bubble columns have irregular shapes. The data from the probe can thus only represent the chord length distribution.

Special attention should be placed on the maximum chord length for the dominant effect of large bubbles on gas holdup. In addition, the measured maximum chord length can be interpreted as

39

the height of the largest bubble (h_{max}) in the system if the number of bubbles detected by the probe is large enough. In general, the maximum bubble height differs from the maximum bubble size. Nevertheless, large bubbles in 2D slurry bubble columns of different solids concentrations have approximately the same maximum dimensions in the horizontal and vertical directions, based on the photos shown by de Swart et al. (1996) and on observations from the 2D experiments. The maximum bubble size can thus be approximated by the maximum bubble height in 2D slurry bubble columns. It is further assumed that this approximation also holds for 3D columns; thus, the maximum bubble chord length is approximated as the maximum bubble diameter in the following analysis.

The maximum bubble size under different conditions is shown in Figure 1. Under otherwise constant conditions, the maximum bubble size decreases with an increase in pressure, especially at pressures lower than 1.5 MPa. Increasing solids concentration leads to significantly larger bubbles at ambient pressure over the entire gas velocity range. On the other hand, at the pressure of 5.6 MPa, the solids concentration has a significant effect on the maximum bubble size only in the gas velocity range of 8–23 cm/s. At gas velocities above that range, the maximum bubble size is virtually independent of solids concentration.

Mechanism of Bubble Breakup

Internal Gas Circulation
An analytical criterion for the bubble breakup can be derived by considering a single large bubble rising in a stagnant liquid at a velocity of u_b, without any disturbances on the gas-liquid interface. The bubble is subjected to breakup when its size exceeds the maximum stable bubble size due to the circulation and centrifugal force. Large bubbles normally assume a spherical cap shape; in this work, the spherical-cap bubble is approximated by an ellipsoidal bubble with the same volume and the same aspect ratio (height to width). The bubble is described in a cylindrical coordinate system that moves with the bubble and has the center of the ellipsoidal bubble as its origin, as shown in Figure 2(a). The bubble surface is formed by rotating an ellipse around the vertical axis, z:

$$\frac{r_c^2}{a^2} + \frac{z^2}{c^2} = 1 \quad (1)$$

$$\frac{r_c^2}{a^2} + \frac{z^2}{c^2} = 1 \qquad\qquad (1)$$

where r_c is the distance from the z axis. The aspect ratio of the ellipse ($\alpha = c/a$) is the same as that of the real spherical cap bubble. The internal circulation can be described by Hill's vortex (Hill, 1894) because of the high Reynolds number of the gas in the bubble. The flow field is symmetrical about the z axis and has no azimuth component. The circulation velocity in the r_c and z directions are, respectively,

$$u = \frac{3u_b}{2c^2} zr_c = \frac{3u_b}{2\alpha^2 a^2} zr_c \qquad\qquad (2a)$$

and

$$w = \frac{3u_b}{2a^2}\left[\left(a^2 - 2r_c^2\right) - \frac{z^2}{\alpha^2}\right]. \qquad\qquad (2b)$$

In the presence of contaminants, a small bubble would behave like a rigid particle and thus, the circulation of the gas inside the bubble could be suppressed. For large bubbles, as encountered in the model, the high shear force generated by the high relative velocity between the bubble and the liquid or slurry could readily sweep away the contaminants on the surface; thus, the contaminants induce negligible effects on the internal circulation of the gas (Levich, 1962).

Evaluation of Centrifugal Force

To model the bubble breakup, it is necessary to evaluate the x-component of the centrifugal force, F_x, on the entire bubble surface, as shown in Figure 2(c). Based on Eqs. (2a) and (2b), there is a surface within the bubble, S, on which the z component of the circulation velocity, w, is zero, and the circulation velocity has only the component in the r_c direction, u, as shown in Figures 2(a) and 2(b). This surface can be described as

$$\frac{2r_c^2}{a^2} + \frac{z^2}{\alpha^2 a^2} = 1. \tag{3}$$

Surface S passes through the vortex center and intercepts all vortex streamlines, as shown in Figure 2(a). Because the pressure field inside the bubble is symmetrical about the x-y plane, F_x is simply the rate of change of momentum across the surface S in the x direction, based on a momentum balance for the gas phase. In addition, the streamlines inside the bubble are symmetrical about the x-y plane and x-z plane, and thus, F_x is four times the rate of the x-component of the gas momentum flowing across an octant of surface S shown in Figure 2(c),

$$F_x = 4 \iint_S \left(\rho_g \vec{u} \cdot \overrightarrow{\delta S} \right) u_x = 4\rho_g \iint_S u^2 \cos\phi \, r_c d\phi dz \tag{4}$$

where $\left(\rho_g \vec{u} \cdot \overrightarrow{\delta S} \right)$ is the mass flow rate across a surface element of S. Substituting Eq. (2a) into Eq. (4) and integrating the resulted equation yields F_x:

$$F_x = 4\rho_g \int_0^{\pi/2} \cos\phi \, d\phi \int_0^c \left(\frac{3u_b z r_c}{2\alpha^2 a^2} \right)^2 r_c dz$$

$$= 4\rho_g \int_0^c \left(\frac{3u_b z r_c}{2c^2} \right)^2 r_c dz = \frac{9\rho_g u_b^2}{\alpha^4 a^4} \int_0^c r_c^3 z^2 dz \tag{4a}$$

From Eq. (3), r_c can be expressed as

$$r_c = \sqrt{\frac{1}{2}\left[a^2 - \left(\frac{z}{\alpha} \right)^2 \right]}. \tag{5}$$

Substituting Eq.(5) into Eq. (4a) and integrating the resulting equation yields F_x:

$$F_x = \frac{9\rho_g u_b^2}{2\sqrt{2}\alpha^4 a^4} \int_0^c z^2 \left[a^2 - \left(\frac{z}{\alpha} \right)^2 \right]^{3/2} dz$$

$$= \frac{9\pi}{64\sqrt{2}\alpha} \rho_g u_b^2 a^2 = \frac{0.312}{\alpha} \rho_g u_b^2 a^2 \tag{6}$$

Criterion of Bubble Breakup

The surface tension force is the product of the surface tension and the circumference of the ellipse,

$$F_\sigma = \sigma L = \sigma \int_{ellipse} \sqrt{(\delta r_c)^2 + (\delta z)^2} = 4\sigma a\, E(\sqrt{1-\alpha^2}) \tag{7}$$

where $E(\sqrt{1-\alpha^2})$ is the complete second kind of elliptic integral that decreases with a decrease in α. Also, the volume equivalent bubble diameter, d_e, is related to a and α by

$$\frac{\pi}{6} d_e^3 = \frac{4\pi}{3}\alpha a^3 \tag{8}$$

or

$$a = \frac{d_e}{\sqrt[3]{8\alpha}}. \tag{8a}$$

Note that the centrifugal force is affected significantly by the aspect ratio of the bubble, as well as by the bubble size and the bubble rise velocity. The bubble is not stable if F_x is larger than the surface tension force, F_σ, i.e.,

$$\frac{0.312}{\alpha}\rho_g u_b^2 \left(\frac{d_e}{\sqrt[3]{8\alpha}}\right)^2 \geq 4\sigma\left(\frac{d_e}{\sqrt[3]{8\alpha}}\right) E(\sqrt{1-\alpha^2}) \tag{9}$$

or

$$u_b^2 d_e \geq \frac{8\alpha^{4/3}\, E(\sqrt{1-\alpha^2})}{0.312}\frac{\sigma}{\rho_g}. \tag{9a}$$

When the centrifugal force is larger than the surface tension force, the bubble should be stretched in the x direction. During the stretching, the aspect ratio, α, becomes smaller while d_e and u_b can be assumed to remain constant. As a result, the centrifugal force increases, the surface tension force decreases, and the bubble stretching becomes an irreversible process. When the bubble is stretched to an extent at which the necking phenomenon occurs, the bubble splits into two smaller bubbles. A sequence of events in the photographs shown in Figure 3 confirms the proposed mechanism of bubble breakup. The bubble images in the figure were obtained at a pressure of 3.5 MPa. It can be seen that bubble stretching during rising takes place from $t = 0$ to 68 ms, and the necking starts at $t = 68$ ms. At $t = 85$ ms, the bubble splits into two smaller bubbles.

Equation (9a) indicates that the breakup of bubbles is dictated by various factors, including bubble size, bubble rise velocity, aspect ratio of the bubble, gas density, and gas-liquid surface tension. In addition to the direct contribution to the centrifugal force as illustrated by Eq. (9a), increasing the bubble size leads to a larger bubble rise velocity and a smaller aspect ratio of the bubble, which both favor bubble breakup. As the pressure increases, the gas density increases and the surface tension decreases; thus, bubbles are less stable.

Evaluation of Maximum Stable Bubble Size

The bubble rise velocity in high-pressure slurries can be calculated by a correlation developed by Luo et al. (1997). The simplified form of that correlation for a large bubble is

$$u_b = \sqrt{\frac{2.8\sigma}{\rho_{sl}d_e} + \frac{g d_e}{2}\frac{\rho_{sl}-\rho_g}{\rho_{sl}}}. \tag{10}$$

Equation (10) has a form similar to the modified Mendelson equation (Mendelson, 1967) of Maneri (1995), except that the slurry density here is replaced with the liquid density in Maneri's equation. By substituting Eq. (10) into Eq. (9a), d_e can be solved from the resulting equation:

$$d_e \geq \sqrt{\frac{2\sigma}{g}\left[\frac{8\alpha^{4/3}\,\mathrm{E}\left(\sqrt{1-\alpha^2}\right)}{0.312\rho_g}\frac{\rho_{ls}}{\rho_{sl}-\rho_g}-\frac{2.8}{\rho_{sl}-\rho_g}\right]} \cong \sqrt{\frac{16\alpha^{4/3}\sigma\,\mathrm{E}\left(\sqrt{1-\alpha^2}\right)}{0.312g\rho_g}} . \qquad (11)$$

Therefore, the maximum stable bubble size is

$$D_{max} \approx 7.16\alpha^{2/3}\,\mathrm{E}(\sqrt{1-\alpha^2})^{1/2}\sqrt{\frac{\sigma}{g\rho_g}} . \qquad (12)$$

The aspect ratio of bubble, α, is related to the wake angle, θ_w, by

$$\alpha = \frac{1-\cos\theta_w}{2\sin\theta_w} \qquad (13)$$

and the wake angle for bubbles in liquids depends on the bubble Reynolds number (Clift et al., 1978),

$$\theta_w = 50 + 190\exp\left(-0.62\,\mathrm{Re}^{0.4}\right). \qquad (14)$$

The wake angle of large bubbles in the liquids can be approximated as 50°, since the Reynolds number is normally high. Hence, the aspect ratio is about 0.21 for the large bubbles in liquids, and $\mathrm{E}(\sqrt{1-\alpha^2})^{1/2}$ is close to unity. For large bubbles rising in liquid-solid suspensions, the aspect ratio is approximated as 0.3 (Fan and Tsuchiya, 1990) and $\mathrm{E}(\sqrt{1-\alpha^2})^{1/2}$ is 1.018. The simplified forms of Eq. (12) are

$$D_{max} \approx 2.53\sqrt{\frac{\sigma}{g\rho_g}} \qquad \text{(for } \alpha = 0.21) \qquad (15a)$$

or

$$D_{max} \approx 3.27\sqrt{\frac{\sigma}{g\rho_g}} \qquad \text{(for } \alpha = 0.3). \qquad (15b)$$

The internal circulation model provides an estimation of the upper limit of the maximum stable bubble size, since the external stresses in the liquid phase are ignored in the model. In actual bubble columns or slurry bubble columns, the observed maximum bubble size should be smaller than the predictions by Eqs. (15a) and (15b).

Prediction Results

Figure 4 compares the experimental data of maximum stable bubble sizes obtained in the present experimental system (Nitrogen-Paratherm NF heat transfer fluid-100 μm glass beads) with the predictions by different models. The experimental data of maximum stable sizes in Figure 4 are approximated by the maximum bubble sizes measured over the entire gas velocity range under the specified pressure, temperature, and solids concentration conditions. The comparison between the predictions and the experimental data indicates that the internal circulation model can reasonably predict the maximum stable bubble size at high pressures in the present system, while the observed effect of pressure on bubble size cannot be explained by the Rayleigh-Taylor instability or the Kelvin-Helmholtz instability. For an air/water system, the prediction by Eq.

(15a) for the maximum stable bubble size is 5.7 cm at 1.5 MPa, while Wilkinson (1991) observed a maximum bubble size of about 3 cm. However, Eqs. (15a) and (15b) over-predict the maximum stable size at ambient pressure, as shown in Figure 4. For an air/water system, the predicted maximum stable bubble size is 22 cm, and the reported value is 13.2 cm. The over-prediction by the internal circulation model at ambient pressure suggests that the bubbles are disintegrated by disturbances in the liquid or slurry through other types of mechanisms, e.g., Rayleigh-Taylor instability (Grace et al., 1978) and Kelvin-Helmholtz instability (Kischa and Kocamustafaogullari, 1989), before the bubble size reaches the value predicted by the internal circulation model. Figure 4 shows that the maximum stable bubble size can be estimated by the internal circulation model at pressures higher than 5 atm; at lower pressures, models based on Rayleigh-Taylor instability or Kelvin-Helmholtz instability should be used. To improve the prediction of the internal circulation model at low pressures, the physical properties of the liquid or the slurry and the external stresses would need to be taken into account.

Based on the internal circulation model, the inertia of the gas and gas-liquid surface tension are the dominant factors dictating the maximum stable bubble size at elevated pressures. The model illustrates an insignificant effect of solids concentration on the maximum bubble size at high pressures, since the stresses in the slurry are ignored in the model. However, at ambient pressure, solids concentration has an indirect effect on the maximum bubble size through variations of the shape or the aspect ratio. The maximum stable bubble size would be larger in the slurry than in the liquid, as exhibited by Eqs. (15a) and (15b). Note that the aspect ratio in the slurry (0.3) is larger than that in the liquid (0.21) for a given pressure at high bubble Reynolds numbers.

Notations
a	Width of ellipse
c	Height of ellipse
d_e	Volume equivalent bubble diameter
D_{max}	Maximum stable bubble size
E	Complete second kind elliptic integral
F_x	x-component of the centrifugal force generated by gas circulation
F_σ	Surface tension force
g	Gravitational acceleration
h_{max}	Height of the largest bubble
L	Circumference of the ellipse
P	System pressure
r_c	Radius in a cylindrical coordinate system
Re	Bubble Reynolds number, $\rho_l d_e u_b / \mu_l$
S	Surface within bubble on which the z-component of the circulation velocity is zero
t	Time
u	r_c-component of the circulation velocity of gas inside a bubble
u_b	Bubble rise velocity
U_g	Gas velocity
u_x	x-component of the circulation velocity of gas inside a bubble
w	z-component of the circulation velocity of gas inside a bubble
z	z-coordinate in a cylindrical coordinate system

Greek letters

α	Aspect ratio of bubbles
ϕ	Azimuthal angle in spherical coordinates or cylindrical coordinates
ρ	Density
θ_w	Wake angle
σ	Gas-liquid surface tension
ϕ_s	Solids concentration
μ	Viscosity

Subscripts

g	Gas phase
l	Liquid phase
sl	Slurry

References

Clift, R., J.R. Grace, and M.E. Weber, *Bubbles, Drops, and Particles*, Academic Press, New York (1978).

de Swart, J.W.A., R.F. van Vliet, and R. Krishna, "Size, Structure and Dynamics of "Large" Bubbles in a Two-Dimensional Slurry Bubble Column," *Chem. Eng. Sci.*, **51**, 4619 (1996).

Fan, L.-S. and K. Tsuchiya, *Bubble Wake Dynamics in Liquids and Liquid-Solid Suspensions*, Butterworth-Heinemann, Stoneham, MA (1990).

Grace, J.R., T. Wairegi, and J. Brophy, "Break-Up of Drops and Bubbles in Stagnant Media," *Can. J. Chem. Eng.*, **56**, 3 (1978).

Hill, M.J.M., "On a Spherical Vortex, " *Phil. Trans. Roy. Soc. London*, **185**, 213 (1894).

Kitscha, J. and G. Kocamustafaogullari, "Breakup Criteria for Fluid Particles," *Int. J. Multiphase Flow*, **15**, 573 (1989).

Levich, V.G., *Physiochemical Hydrodynamics*, Prentice Hall, Englewood Cliffs, NJ (1962).

Liu W., N.N. Clark, and A.I. Karamavruc, "General Method for the Transformation of Chord-Length Data to a Local Bubble-Size Distribution," *AIChE J.*, **42**, 2713 (1996).

Luo, X., J. Zhang, K. Tsuchiya, and L.-S. Fan, "On the Rise Velocity of Bubbles in Liquid-Solid Suspensions at Elevated Pressure and Temperature," *Chem. Eng. Sci.*, **52**, 3693 (1997).

Maneri, C. C., "New Look at Wave Analogy for Prediction of Bubble Terminal Velocities," *AIChE J.*, **41**, 481 (1995).

Mendelson, H. D., "The Prediction of Bubble Terminal Velocities from Wave Theory," *AIChE J.*, **13**, 250 (1967).

Wilkinson, P.M., *Physical Aspects and Scale-Up of High Pressure Bubble Columns*, Ph.D. thesis, University of Groningen, The Netherlands (1991).
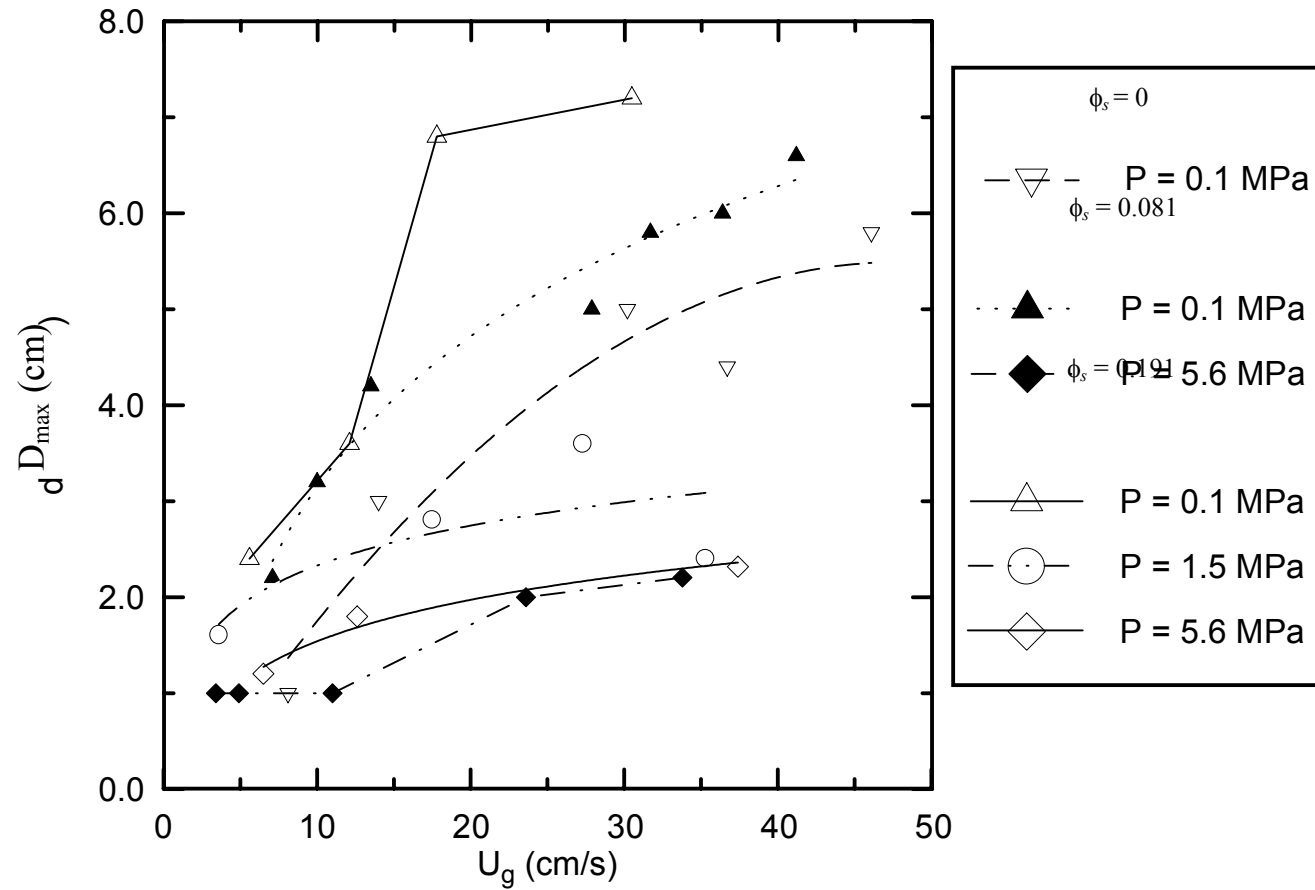
Figure 1. Effects of Pressure and Solids Concentration on the Maximum Bubble Size in a Slurry Bubble Column ($T = 78ºC$)
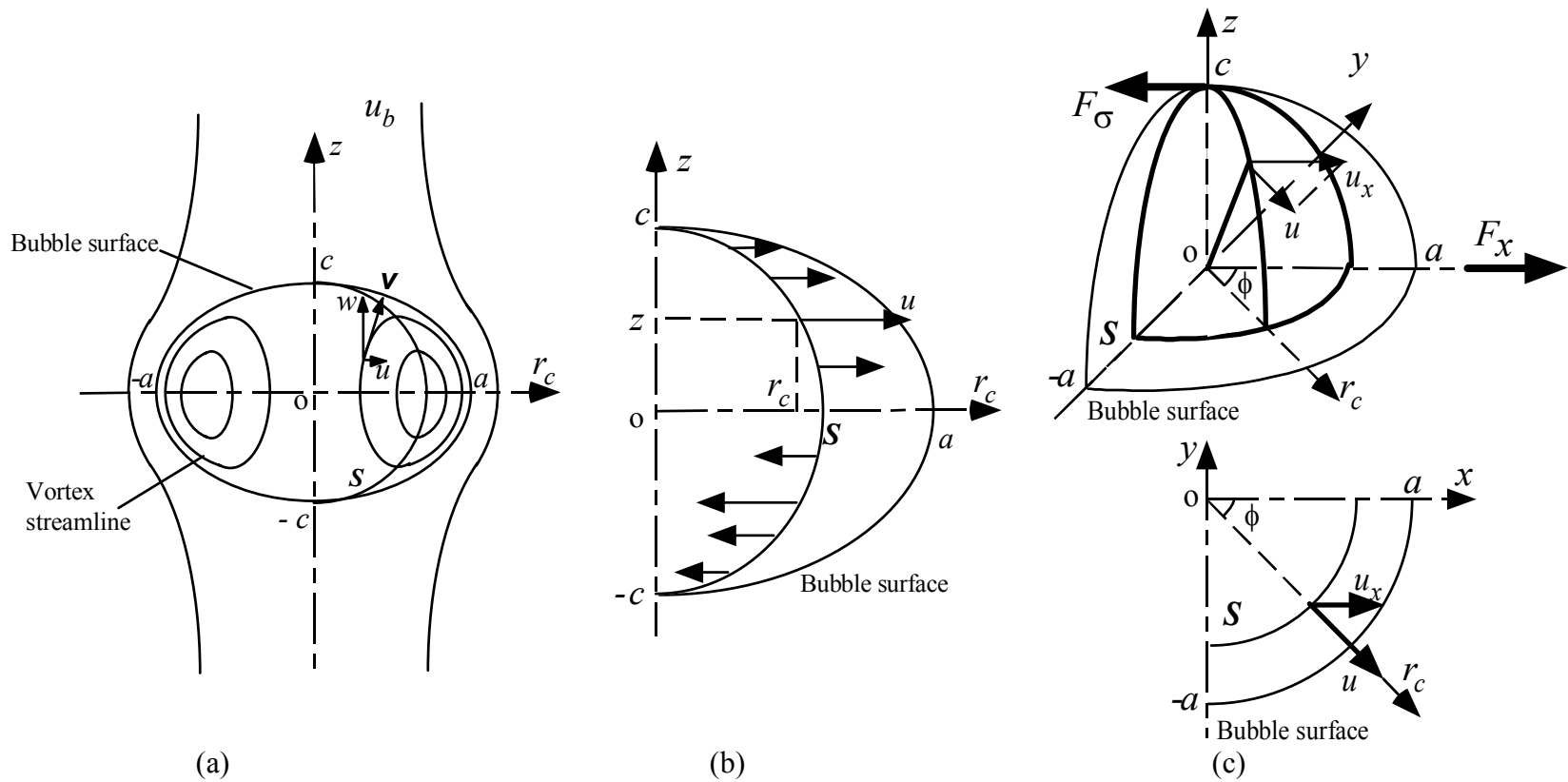
Figure 2. Schematic of the Internal Circulation Model for Bubble Breakup: (a) Internal and External Flow Fields; (b) Circulation Velocity on Surface S; (c) Force Balance and 3D View of Surface S and the Flow Pattern on S

(a) t = 0 ms   (b) t = 17 ms   (c) t = 34 ms

(d) t = 51 ms   (e) t = 68 ms   (f) t = 85 ms
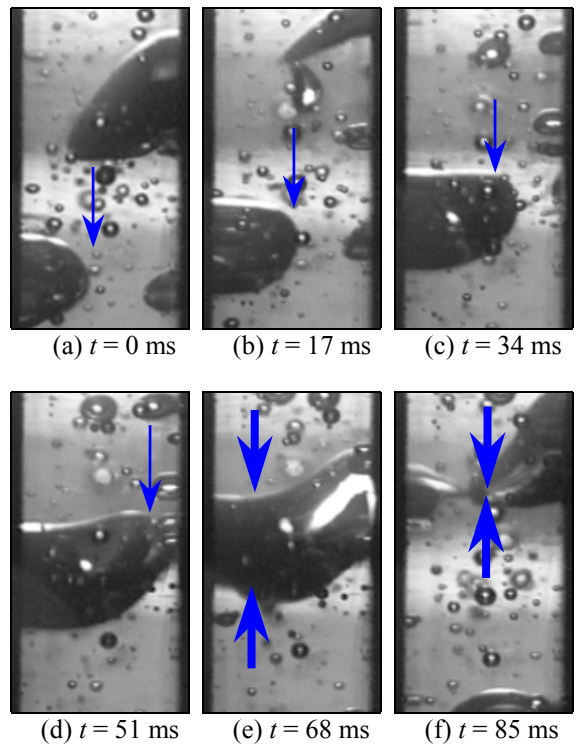
Figure 3. A Sequence of Bubble Images Showing the Process of Bubble Breakup
(P = 3.5 MPa)
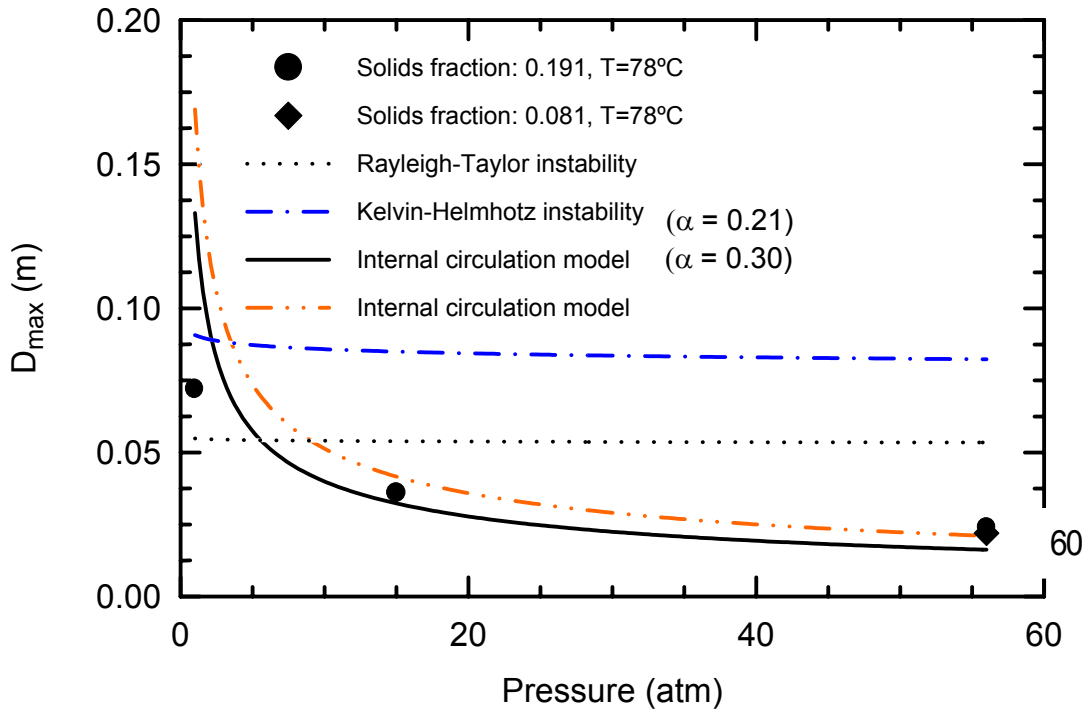
Figure 4. Comparison of the Maximum Stable Bubble Size Between the Experimental Data and the Predictions by Different Models